Measurement Matrix Calibration Method for Modulated Wideband Converter under Imperfect Periodic Pseudorandom Waveform

Tianyi Xiong, Zan Li, and Peihan Qi
School of Telecommunications Engineering, Xidian University, Xi'an 710071, China
Email: xiongtianyi89@gmail.com; {zanli, phqi}@xidian.edu.cn

Abstract —Modulated Wideband Converter (MWC) is a type of practical Compressed Sensing (CS) framework that bridges CS theory to real-time sub-Nyquist sampling and recovery of sparse wideband analog signal with low computational overhead and efficient hardware implementation. However, the application and implementation of MWC are seriously disturbed by the measurement matrix mismatch problem caused by limited system bandwidth and inevitable nonlinearity of practical devices. To remit this awkwardness, a Full-column-rank Well-Posed Calibration (FWC) method aiming to calibrate measurement matrix of MWC is proposed in this paper. By controlling the number and carrier frequency of input analog signal, the underdetermined reconstruction problem is turned to be well-posed equation set which is solved iteratively and then the calibration of the measurement matrix is completed. Theoretical analysis and numerical simulation results indicate that the measurement matrix obtained by proposed method keeps a high accordance with the theoretical value and adapts to the practical MWC system, thus ensuring the recovery accuracy of the original signal.

Index Terms—Compressed sensing, modulated wideband converter, measurement matrix, calibration

I. Introduction

Since the establishment, classical Shannon-Nyquist sampling theorem [1], [2] has been one of most pivotal foundations of communication and signal processing. It points out that a low-pass continuous-time signal must be discretized with a sampling rate at least the twice of the maximal frequency for the sake of undistorted reconstruction meanwhile band-pass analog signal requires a minimal sampling rate twice of its bandwidth and the corresponding sampling frequency is constrained within a range determined by the minimal and the maximal component. In the past decades, evolving wireless service and applications result in the ever-increasing data types, high throughput and transmission rate, which brings about the significant expanding in occupied frequency bandwidth [3]-[5]. This demands excellent performance analog to digital converter (ADC), huge storage and logical device with high-speed processing ability, raising new challenges and bottleneck problems to the orthodox digital signal processing mechanism based on conventional sampling theorem. Fortunately, with the help of convex optimization techniques, Compressed Sensing (CS) theorem [6]-[8], with a very high probability, is able to perfectly recover the original analog signal that is sparse in some transform domain with only very few non-adaptive, linear measurements. Consequently, CS theory offers new theoretical foundation and practical application for alleviating the pressure on ADC performance and the DSP processing speed, making it much easier and more feasible to realize the conversion from wideband analog signal to digital information without harsh requirements in hardware.

Since the emerging of CS theory, huge efforts has been devoted to the practical implementation of CS theory and several CS sampling framework has been proposed which includes Random Demodulator (RD) [9], [10], random convolution converter (RC) [11], wideband filter bank converter [12], Modulated Wideband Converter (MWC) [13]-[16]. RD, which adopts finite and discrete multi-tone signal as the analog input model, first multiplies the input by a random sequence and then the product is integrated and low-pass sampled to obtain the compressed measurements. This framework can be easily realized in practice but is sensitive to reconstruction error caused by the mismatch problem of input model in the case of recovering a signal with continuous spectrum within ultra wideband. However, accurate input model will suffer the predicament of high dimension and complex matrix computational load [10]. RC convolves the input analog signal with a FIR filter equipped with random tap coefficients and then acquires compressed measurement via decimation [11]. This kind of compressed sampling scheme settles the problem of real-time recovery that is barely possible for RD but does not make any improvement in the analog input model and brings the new trouble of high-speed convolution implementation. Wideband filter bank converter employs a group of random chips, a mixer and a bank of quadrature mirror filter to avoid the cost of the multiple branch hardware in MWC and overcome the difficulty in choosing multiple random chips [12]. Nevertheless, it overlooks the

Manuscript received November 27, 2015; revised May 14, 2016.
This work was supported by the National Natural Science Foundation of China under Grant No. 61501356.
Corresponding author email: phqi@xidian.edu.cn.
doi:10.12720/jcm.11.5.498-506

hardship in designing filter with high Q-factor value and the input bandwidth limitation of commercial ADC. MWC [13]-[16] takes the union of subspaces which are provided with the shift invariance property as the input model and multiplies the analog signal by a bank of periodic random sequence in multiple branches. This completes the decomposition of the original input signal in subspace and significantly reduces the necessary sampling rate. Afterward, by detecting the occupied subspaces, continuous spectrum signals without any aliasing and short time pulse with any kind of waveforms can be compressed sampled and reconstructed in real-time. In general, the MWC framework is an efficient, tractable and low cost approach to analyze wideband sparse signal and is a kind of analog information converter that is the most extensively studied by now.

However, the designing and hardware implementation of MWC could be easily affected by the limitation of system bandwidth and some other nonlinear factors [16], [17]. To be specific, the waveform of the periodic pseudorandom sequence would hardly be perfect square waveform, the pass band of wideband mixer and low-pass filter will not be as flat as required and the frequency response of low-pass filter has an inevitable transitional zone. All these undesirability will result in the mismatch problem of the measurement matrix for sampling and reconstruction and will greatly reduce the accuracy of signal recovering. Among the existing literatures addressing these imperfect elements, the author of reference [16] eliminated the influence of the fluctuant within the pass band of the mixer by pre-equalizer and controlling the power of local oscillator. Reference [17] deduced the conditions of perfect recovery with general filter and used FIR filter to compensate the imperfection in pass band and the trailing in transition zone of low-pass filter. To the best of our knowledge, there are not any techniques aiming at calibrating the error brought by non-ideal periodic pseudorandom sequence so far. Inspired by this, we proposed a Full-column-rank Well-Posed Calibration (FWC) method to overcome the mismatch problem of the measurement matrix in MWC caused by the defective periodic pseudorandom waveform. By FWC method, the measurement matrix used in the step of compressed sampling and reconstruction is adjusted to adapt the practical hardware implementation, which ensures the accuracy of signal recovery.

The rest of this paper is organized as follows. Section II briefly introduces the principles of MWC compressed sampling system. Section III explained how the mismatch problem of measurement matrix in MWC framework comes. The technological process and the theory analysis of FWC method are presented in Section IV. Section V displays the computer numerical simulation results with corresponding descriptions and the last section concludes the whole work of paper.

II. Modulated Wideband Converter

For the convenience of describing the mismatch problem of the measurement matrix in subsequent sections, we briefly review the principle of MWC framework and the process of obtaining the measurement matrix under ideal conditions in this section.

A. MWC Principles

The block diagram of MWC compressed sampling framework [13] is depicted in Fig. 1. The input ultra wideband signal $x_0(t)$ is divided by a power divider the output of which enter m channels simultaneously and each of them is multiplied by a Rademacher sequence $p_i(t), i=1,2,...,m$ (i.e. ± 1 sequence with equal chance) with period of T_p. To avoid aliasing, each product is then filtered by ideal low-pass $h(t)$ whose pass band is $[0,1/2T_s]$. After that, the output of filters are uniformly sampled at the rate of $f_s = 1/T_s$, and compressed samples $y_i(n), i=1,2,...,m$, $n=0,1,2...$ can be obtained. By means of frame construction and multiple measurement vectors problem solution, original signal can be estimated from low-rate digital signal processing.

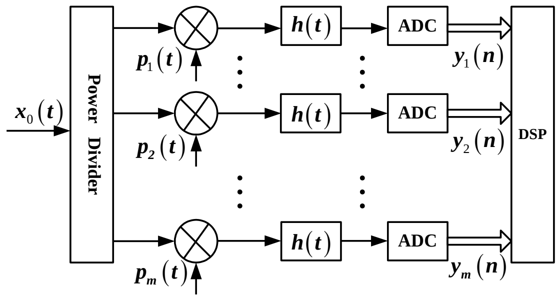

Fig. 1. MWC block diagram

Assume that the input original signal to the MWC module is denoted as $x_0(t) = \sqrt{m}x(t)$, then the output of the power divider in each branch is $x(t)$. After mixed by Rademacher sequence and filtered by anti-aliasing filter, we have

$$y_i(t) = \int_{-\infty}^{\infty} x(\tau)p_i(\tau)h(t-\tau)d\tau, i=1,2,...,m. \quad (1)$$

The discrete points after low-pass sampling are

$$y_i(n) = y_i(t)\big|_{t=nT_s}, n=0,1,..., \quad (2)$$

Due to the periodicity of $p_i(t)$, the discrete time Fourier transform can be written as

$$Y_i(f) = \sum_{l=-\infty}^{\infty} c_{il} X(f - lf_p), f \in [-f_s/2, f_s/2]. \quad (3)$$

where c_{il} is the Fourier coefficient of $p_i(t)$, $f_p = 1/T_p$ is the reciprocal of the period of the random chips and

$X(f)$ is the continuous Fourier transformation of $x(t)$. By using the equivalent Nyquist sampling rate f_{NYQ} of MWC, f_p and f_s, the number of the subspaces which are necessary to represent $X(f)$ integrality is

$$L = 2L_0 + 1, L_0 = \left\lceil \frac{f_{NYQ} + f_s}{2f_p} \right\rceil - 1 \tag{4}$$

Define vectors

$$\mathbf{Y}(f) = \left[Y_1(f), \ldots, Y_i(f), \ldots, Y_m(f)\right]^T,$$

$$\mathbf{Z}(f) = \left[Z_1(f), \ldots, Z_l(f), \ldots, Z_L(f)\right]^T.$$

where $Z_l(f) = X\left(f + (l - L_0 - 1) f_p\right)$, $1 \le l \le L$, and $f \in \left[-f_s/2, f_s/2\right]$. Notice that $\mathbf{Z}(f)$ is sparse if the original input signal only occupies minority spectrum source within the ultra wideband range.

Then equation (3) can be simplified as

$$\mathbf{Y}(f) = \mathbf{AZ}(f). \tag{5}$$

Here $\mathbf{A}$ is the so-called measurement matrix whose entries are $\mathbf{A}_{il} = c_{i,-l} = c_{il}^*$, symbol $*$ denotes the function of complex conjugate.

Define another vector consisting of discrete samples from each branch as

$$\mathbf{y}(n) = \left[y_1(n), \ldots, y_i(n), \ldots, y_m(n)\right]^T$$

and its correlation matrix can be calculated as

$$Q = \int_{-f_s/2}^{+f_s/2} y(f) y^H(f) df = \sum_{n=-\infty}^{\infty} y(n) y^T(n) \tag{6}$$

After decomposing this correlation matrix as $\mathbf{Q} = \mathbf{VV}^H$, the multiple measurement vectors (MMV) problem is formulated as follows by adopting matrix $\mathbf{V}$ and $\mathbf{A}$

$$\mathbf{V} = \mathbf{AU} \tag{7}$$

And then the support set $S = \operatorname{supp}(\bar{\mathbf{U}})$ of $\mathbf{Z}(f)$ can be recovered, where $\bar{\mathbf{U}}$ is a sparse matrix regenerated by orthogonal matching pursuit (OMP) algorithm from equation (7). Finally, the analog signal $x(t)$ can be reconstructed from the following expressions.

$$\mathbf{z}_S[n] = \mathbf{A}_S^{\dagger} \mathbf{y}[n] \tag{8a}$$

$$z_i[n] = 0, \quad i \notin S \tag{8b}$$

$$x(t) = \sum_{i \in S, i \ge 0} \Re\{z_i(t)\} \cos(2\pi i f_p t) + \mathrm{I}\{z_i(t)\} \sin(2\pi i f_p t). \tag{8c}$$

where $\mathbf{A}_S^{\dagger} = \left(\mathbf{A}_S^H \mathbf{A}_S\right)^{-1} \mathbf{A}_S^H$, $\mathbf{z}(n) = \left[z_1(n), \ldots, z_L(n)\right]^T$ and $z_i(t)$ is complex and the output of a low-pass filter which has the cutoff frequency $f_s/2$ and is stimulated by $z_i(n)$.

B. *Measurement Matrix Computation*

From equations (5), (7) and (8), we know that the measurement matrix used to compressed sampling and the one used to reconstruction in MWC framework should be highly consistent or the reconstructed signal will be seriously affected and distorted. Generally, the voltage amplitude, occupied bandwidth, in-band power and some other practical factors of the periodic pseudorandom chips $p_i(t)$ are not taken into consideration in the theoretical analysis of the previous literatures. The pseudorandom chips $p_i(t)$ are treated as ideal -1 and +1 sequence shown in Fig. 2(a).

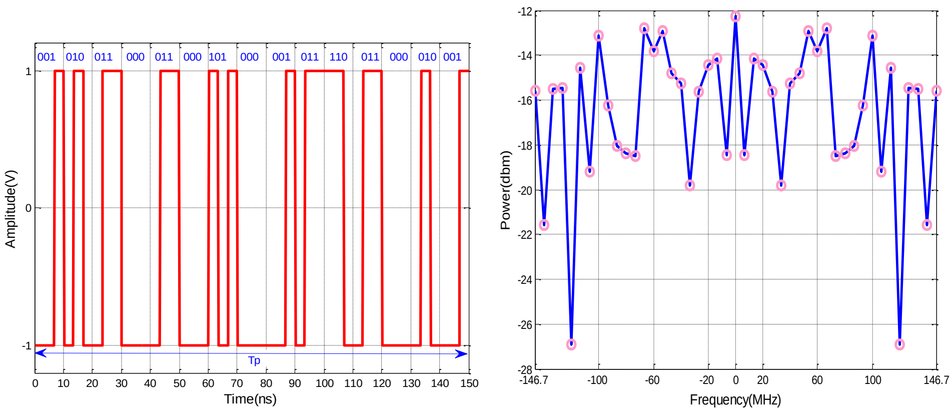

(a) (b)

Fig. 2. Waveforms of ideal pseudorandom sequence: (a) time domain waveform; (b) frequency domain waveform

If the number of chips in sequences is denoted as L, $p_i(t)$ can be regarded as the sum or difference of L unit step-function, the measurement matrix $\mathbf{A}$ can be worked out by considering the periodicity of $p_i(t)$, and its Fourier series coefficients can be expressed as

$$
\begin{aligned}
c_{il} &= \frac{1}{T_p}\int_0^{T_p}\sum_{k=0}^{L-1}\alpha_{ik}\left(u\left(t-\frac{kT_p}{L}\right)-u\left(t-\frac{(k+1)T_p}{L}\right)\right)e^{-j\frac{2\pi}{T_p}lt}dt \\
&= \frac{1}{T_p}\sum_{k=0}^{L-1}\alpha_{ik}\int_0^{T_p}\left(u\left(t-\frac{kT_p}{L}\right)-u\left(t-\frac{(k+1)T_p}{L}\right)\right)e^{-j\frac{2\pi}{T_p}lt}dt \\
&= \frac{1}{T_p}\sum_{k=0}^{L-1}\alpha_{ik}\int_{\frac{kT_p}{L}}^{\frac{(k+1)T_p}{L}} e^{-j\frac{2\pi}{T_p}lt}dt\left(t^{'}=t-\frac{kT_p}{L}\right) \\
&= \frac{1}{T_p}\sum_{k=0}^{L-1}\alpha_{ik}e^{-j\frac{2\pi}{L}lk}\int_0^{\frac{T_p}{L}} e^{-j\frac{2\pi}{T_p}lt}dt \\
&= d_l\sum_{k=0}^{M-1}a_{ik}\theta^{lk}
\end{aligned}
\tag{9}
$$

where $\theta=\exp(-j2\pi/L)$, $d_l=\frac{1}{T_p}\int_0^{\frac{T_p}{L}}\exp\left(-j\frac{2\pi}{T_p}\right)dt$,

then the measurement matrix $\mathbf{A}$ is written as

$$
A=\underbrace{\begin{bmatrix}\alpha_{1,0} & \cdots & \alpha_{1,L-1}\\ \vdots & \ddots & \vdots\\ \alpha_{m,0} & \cdots & \alpha_{m,M-1}\end{bmatrix}}_{\mathbf{S}}
\times\underbrace{\begin{bmatrix}| & \cdots & | & \cdots & |\\ \overline{F}_{L_0} & \cdots & \overline{F}_0 & \cdots & \overline{F}_{-L_0}\\ | & \cdots & | & \cdots & |\end{bmatrix}}_{\mathbf{F}}
\times\underbrace{\begin{bmatrix}d_{L_0} & & \\ & \ddots & \\ & & d_{-L_0}\end{bmatrix}}_{\mathbf{D}}
\tag{10}
$$

In equation (10), $\mathbf{S}$ is a sign matrix with the dimension of $m\times L$, and the column vector $\overline{F_i}=\left[1,\theta^{i},\theta^{2i}...,\theta^{(L-1)i}\right]^T$, matrix $\mathbf{D}=diag\left(d_{L_0},...,d_{-L_0}\right)$.

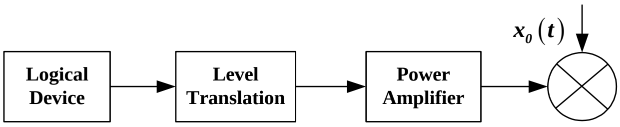

Fig. 3. Pseudorandom sequence generator

TABLE I: PARAMETERS OF SEQUENCE GENERATOR

Items	Parameters
Logical Device	XC3S100E (Xilinx FPGA)
Interface Level	LVDS
Level Converter	TC4-1W
Power Amplifier	GALI-84
Sequence Period	150 ns
Used Sequence	0010100110000110001010000010111100110000100 01

III. MISMATCH PROBLEM OF MEASUREMENT MATRIX

In practice, a common way to generate high speed pseudorandom random wave form is to use logical element such as shifting register to output pseudorandom 0 and 1 sequence and then convert these symbols to standard interface level followed by power amplifier to get a proper level to meet the requirement of mixer. As shown in Fig. 3, the hardware of sequence generator is implemented in this piece of work and the components used and parameter set are described in Table I. Firstly, to ensure the alternation rate of 300 mega bits per second, logical device XC3S100E is designed to shift out 0 or 1 symbol with LVDS interface level, then level converter TC4-1W transformed the sequence from LVDS to single-ended. Finally, the power amplifier Gali-84 magnified the pseudorandom waveform as the mixer needed.

Due to the limited system bandwidth and the non-linear character of wideband power amplifier, the pseudorandom sequence used to mix the original input cannot be strictly square wave. The actual waveform and its power spectrum density after level switch and power amplifying are plotted in Fig. 4. It should be pointed out that the waveform is plotted with the data sampled by oscilloscope.

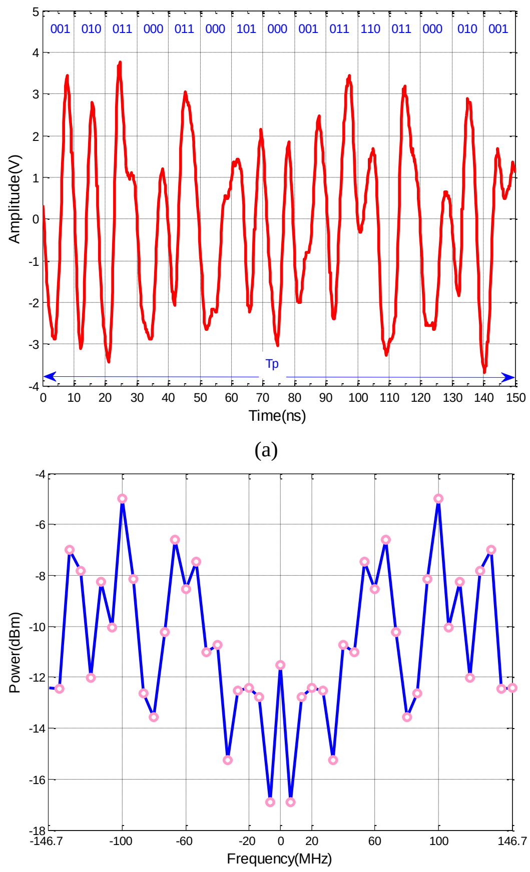

(a)

(b)

Fig. 4. Waveforms of real pseudorandom sequence: (a) time domain waveform; (b) frequency domain waveform

By comparing Fig. 4(a) with Fig. 2(a), it is apparent that the periodic pseudorandom sequence has been smoothed or distorted that is there are no sharp rising and falling at the edge of a chip which resulted from limited system bandwidth. The rising time and falling time of the waveform vary with different device and clock frequency [18]. On the other hand, to be strong enough to drive the mixer, the sequence should be amplified but non-linearity of power amplifier could lead to serious overshoot and ringing in the waveform of periodic pseudorandom sequence. MWC framework needs to amplify multi-tone signal in an ultra wideband which is different from conventional single-tone amplification, which will certainly bring further distortion in pseudorandom sequence waveform due to the non-linear amplification. All these non-ideal factors discussed above in time domain waveform would affect the value of Fourier series coefficients.

To be more convinced, turn to Fig. 4(b) and Fig. 2(b) and we can see that the level difference of two discrete frequency point -60MHz and -100MHz is 3.75dB in Fig. 4(b) while the level difference of the same frequency point is 0.7dB in Fig. 2(b). All these variations in power level will be embedded in the fluctuation of the measurement matrix entries. So far, based on the analysis and experiment, the measurement matrix depends on not only specific periodic pseudorandom sequence but also other inherent non-ideal factors. Hence it can be concluded that it will certainly bring about the mismatch problem if we employ the method described in subsection B of section II to obtain measurement matrix.

IV. Full-Column-Rank Well-Posed Calibration Method

This section presented the proposed FWC algorithm aiming to overcome the measurement matrix mismatch problem in practical implementation of MWC framework.

A. The Procedure of FWC Method

The flow diagram of FWC method calibrating the measurement matrix is depicted in Fig. 5. A signal output from vector signal generator is divided into two components by a power divider which are fed into MWC compressed sampling system and a super heterodyne receiver respectively. Afterwards, the calibration will be realized with the following steps.

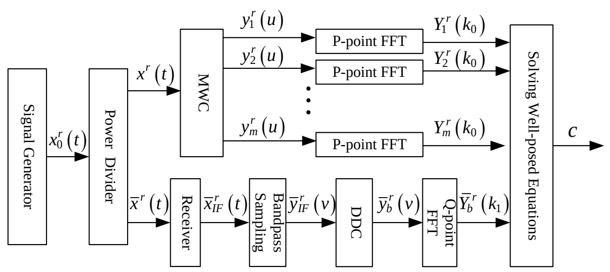

Fig. 5. Block diagram of FWPC algorithm

(a) Initial the times of switching frequency point of generator as $r=0$ and the measurement matrix to calibrate $\bar{\mathbf{A}}=\mathbf{0}$ with the dimension of $m\times L$;

(b) Set the vector signal generator to output a digital modulated signal $x_0^r(t)$ with carrier $f_c = rf_p$, $0<r<L_0$. After power divider, the signal input to MWC is denoted as $x^r(t)$ and the other identical component input to super heterodyne receiver denoted as $\bar{x}^r(t)$ is tuned to an intermediate frequency signal $\bar{x}_{IF}^r(t)$ by up or down conversion;

(c) Acquire $x^r(t)$ and $\bar{x}_{IF}^r(t)$ synchronously and adopt the output of the m sampling channel to form a vector $\mathbf{y}^r(u)=\left[y_1^r(u), y_2^r(u),..., y_m^r(u)\right]^T$, $0\le u\le P-1$. And the output of the band pass sampler is $\bar{y}_{IF}^r(v)$, $0\le v\le Q-1$, the band pass sampling rate satisfies $f_s^{'}=Qf_s/P$;

(d) Conduct P-point Fast Fourier Transform (FFT) on the MWC output of each channel $y_i^r(u)$, $1\le i\le m$ and obtain another group of vectors those are $\mathbf{Y}^r(k_0)=[Y_1^r(k_0),...,Y_i^r(k_0),...,Y_m^r(k_0)]^T$, $1\le i\le m$ and the frequency index $0\le k_0\le P-1$.

(e) Modulate intermediate frequency samples $\bar{y}_{IF}^r(v)$ to baseband signal $\bar{y}_b^r(v)$ via digital quadrature down conversion and perform Q points FFT obtaining $\bar{Y}_b^r(k_1)$, where $0\le k_1\le Q-1$, and also $\left[\bar{Y}_b^r(-k_1)\right]^*$ by linear operation;

(f) Solve the well-posed equations set composed of $\mathbf{Y}^r(k_0)$, $\bar{Y}_b^r(k_1)$ and $\left[\bar{Y}_b^r(-k_1)\right]^*$ to obtain one column vector $\mathbf{c}$ of measurement matrix, the solving procedures will be given in the next subsection.

(g) In the case $r=0$, we let $\bar{\mathbf{A}}(:,L_0+1)=\mathbf{c}$; If $0<r<L_0$, we let $\bar{\mathbf{A}}(:,L_0+r+1)=\mathbf{c}$ and $\bar{\mathbf{A}}(:,r)=\mathbf{c}^*$

Update $r=r+1$ and repeat from step (b) to step (f); In the case $r=L_0$, let $\bar{\mathbf{A}}(:,L_0+r+1)=\mathbf{c}$ and $\bar{\mathbf{A}}(:,r)=\mathbf{c}^*$. Finally, the calibration of measurement matrix $\bar{\mathbf{A}}$ is accomplished.

B. Theoretical Analysis

First of all, we assume that the signal $x(t)$ input to the MWC framework is the modulated version of the baseband signal $x_b(t)=I_b(t)+jQ_b(t)$ by quadrature up conversion as follows

$$\begin{aligned} x(t) &= I_b(t)\cos(2\pi f_c t) - Q_b(t)\sin(2\pi f_c t) \\ &= I_b(t)\frac{e^{j2\pi f_c t}+e^{-j2\pi f_c t}}{2} - Q_b(t)\frac{e^{j2\pi f_c t}-e^{-j2\pi f_c t}}{2j} \\ &= \frac{I_b(t)+jQ_b(t)}{2}e^{j2\pi f_c t} + \frac{I_b(t)-jQ_b(t)}{2}e^{-j2\pi f_c t} \\ &= \frac{x_b(t)}{2}e^{j2\pi f_c t} + \frac{x_b^*(t)}{2}e^{-j2\pi f_c t}. \end{aligned} \tag{11}$$

According to the frequency-shift property of Fourier transform, the Fourier transform of $x(t)$ is given by

$$X(f)=\frac{1}{2}X_b(f-f_c)+\frac{1}{2}X_b^*(-f-f_c). \tag{12}$$

where $X_b(f)$ is the Fourier transform of $x_b(t)$, and the Fourier transform of $\tilde{x}_i(t)$ which is the product of $x(t)$ and the periodic pseudorandom waveform $p_i(t)$ is derived by

$$\begin{aligned}\tilde{X}_i(f) &= \int_{-\infty}^{\infty} \tilde{x}_i(t) e^{-j2\pi ft} dt \\ &= \int_{-\infty}^{\infty} x(t)\left(\sum_{l=-\infty}^{\infty} c_{il} e^{j\frac{2\pi}{T_p}lt}\right) e^{-j2\pi ft} dt \\ &= \sum_{l=-\infty}^{\infty} c_{il} X(f - lf_p).\end{aligned} \tag{13}$$

Let $\tilde{X}_i(f)$ go through a low-pass filter and consider the equivalent Nyquist sampling rate of the MWC and (13) can be written in matrix form as

$$\underbrace{\begin{pmatrix} Y_1(f) \\ Y_2(f) \\ \vdots \\ Y_m(f) \end{pmatrix}}_{\mathbf{y}(f)} = \underbrace{\begin{bmatrix} c_{1,1}^* & \cdots & c_{1,L}^* \\ \vdots & \ddots & \vdots \\ c_{m,1}^* & \cdots & c_{m,L}^* \end{bmatrix}}_{\mathbf{A}} \underbrace{\begin{pmatrix} X(f - L_0 f_p) \\ \vdots \\ X(f) \\ \vdots \\ X(f + L_0 f_p) \end{pmatrix}}_{\mathbf{z}(f)} \tag{14}$$

where $-f_s/2 \le f \le f_s/2$. Assuming $f_c = rf_p$, $f_s = f_p$, $0 \le r \le L_0$, $r \in \mathbb{Z}$, we can easily imply from equation (12) and (14) that only the spectrum component within $X(f + rf_p)$ and $X(f - rf_p)$ can be shifted into the band range $[-f_s/2, f_s/2]$. Consequently equation (14) is simplified as

$$\begin{cases} Y_1(f) = \frac{1}{2} c_{1,r} X_b(f) + \frac{1}{2} c_{1,r}^* X_b^*(-f) \\ Y_2(f) = \frac{1}{2} c_{2,r} X_b(f) + \frac{1}{2} c_{2,r}^* X_b^*(-f) \\ \vdots \\ Y_m(f) = \frac{1}{2} c_{m,r} X_b(f) + \frac{1}{2} c_{m,r}^* X_b^*(-f) \end{cases} \tag{15}$$

Define

$$X_{b+}(f) \triangleq \frac{1}{2}\left[X_b(f) + X_b^*(-f)\right]$$

$$X_{b-}(f) \triangleq \frac{1}{2}\left[X_b(f) - X_b^*(-f)\right]$$

and equation (15) can be written as

$$\begin{cases} Y_1(f) = \left[\mathcal{R}(X_{b+}(f))\mathcal{R}(c_{1,r}) - \mathcal{I}(X_{b-}(f))\mathcal{I}(c_{1,r})\right] \\ \quad + j\left[\mathcal{I}(X_{b+}(f))\mathcal{R}(c_{1,r}) + \mathcal{R}(X_{b-}(f))\mathcal{I}(c_{1,r})\right] \\ Y_2(f) = \left[\mathcal{R}(X_{b+}(f))\mathcal{R}(c_{2,r}) - \mathcal{I}(X_{b-}(f))\mathcal{I}(c_{2,r})\right] \\ \quad + j\left[\mathcal{I}(X_{b+}(f))\mathcal{R}(c_{2,r}) + \mathcal{R}(X_{b-}(f))\mathcal{I}(c_{2,r})\right] \\ \vdots \\ Y_m(f) = \left[\mathcal{R}(X_{b+}(f))\mathcal{R}(c_{m,r}) - \mathcal{I}(X_{b-}(f))\mathcal{I}(c_{m,r})\right] \\ \quad + j\left[\mathcal{I}(X_{b+}(f))\mathcal{R}(c_{m,r}) + \mathcal{R}(X_{b-}(f))\mathcal{I}(c_{m,r})\right] \end{cases} \tag{16}$$

where $\mathcal{R}(\cdot)$ and $\mathcal{I}(\cdot)$ denotes taking real part and image part respectively. Obviously, equation (16) is a well-posed equation set, and each complex equation can be split into two real equations. Then by solving this equation set, we get $\mathbf{c} = [c_{1,r}, ..., c_{i,r}, ..., c_{m,r}]^T$, which is one column of the calibrated measurement matrix $\bar{\mathbf{A}}$. And the real part and image part of $c_{i,r}$ respectively are

$$\begin{cases} \mathcal{R}(c_{i,r}) = \dfrac{\mathcal{R}(X_{b-}(f))\mathcal{R}(Y_i(f)) + \mathcal{I}(X_{b-}(f))\mathcal{I}(Y_i(f))}{\mathcal{R}(X_{b+}(f))\mathcal{R}(X_{b-}(f)) + \mathcal{I}(X_{b+}(f))\mathcal{I}(X_{b-}(f))} \\ \mathcal{I}(c_{i,r}) = \dfrac{\mathcal{R}(X_{b+}(f))\mathcal{I}(Y_i(f)) - \mathcal{I}(X_{b+}(f))\mathcal{R}(Y_i(f))}{\mathcal{R}(X_{b+}(f))\mathcal{R}(X_{b-}(f)) + \mathcal{I}(X_{b+}(f))\mathcal{I}(X_{b-}(f))} \end{cases} \tag{17}$$

V. Performance Simulation and Analysis

Numerical simulation of FWC algorithm based on practical MWC compressed sampling system is conducted in this section. The calibrated elements of the measurement matrix obtained by the proposed method are used to reconstruct the original signal and the correct recovery ratio of the support set is also analyzed and depicted.

A. Calibrated and Theoretical Value of Measurement Matrix

Assume that the equivalent Nyquist sampling rate of MWC framework which we want to calibrate is $f_{NYQ} = 300\text{MHz}$, the number of sampling channel is $m = 1$, the period and frequency of pseudorandom sequence shown in Fig. 4(a) are $T_p = 0.15\text{us}$ and $f_p = 6.67\text{MHz}$ respectively. The number of chips in one cycle is $L = 45$. The low pass sampling rate of each channel is $f_s = 6.667\text{MHz}$. According to the procedure of FWC method given in subsection A of IV, a BPSK signal is generated with carrier $f_c = rf_p$ each time r is an integer that varies from 0 to 23 and the symbol rate of modulated signal is set as $s_r = 1\text{Mbaud}$. The number of samples acquired by MWC compressed system is fixed as $N = 36000$.

Table II presented the elements of measurement matrix obtained from theoretical computation and practical calibration. Specifically, the theoretical computational value is the result of FFT on the periodic pseudorandom waveform depicted in Fig. 4(a) while the practical calibration value is achieved by FWC method. Since the number of sampling channel is set as 1 and accordingly the dimension of measurement matrix is 1×45, table 2 only lists 23 elements of it due to the conjugate symmetry property of this matrix.

Table II shows that the elements of measurement matrix obtained by FWC method are highly consistent with those from theoretical computation. The estimation error between the two different processes is controlled less than 1%, which satisfies the requirement in most scenes. It's worth noting that although the theoretical computation value can be obtained by theorem, this method has its inherent limitation compared with FWC method since both non-linearity in mixer and fluctuation in low-pass filter will distort the real value of the elements of measurement matrix whereas the periodic pseudorandom waveform output from the mixer and low-pass filter cannot be test in practice. On the contrary, FWC method regards MWC framework as a whole entirety which makes it possible to complete the calibration of measurement matrix precisely.

TABLE II: CALIBRATED VALUE AND THEORETICAL VALUE

item	Calibrated value	Theoretical value	item	Calibrated value	Theoretical value
$A_{1,1}$	0.019+j0.120	0.019+j0.120	$A_{1,13}$	0.126-j0.446	0.125-j0.447
$A_{1,2}$	0.096+j0.072	0.096+j0.072	$A_{1,14}$	0.122-j0.270	0.121-j0.271
$A_{1,3}$	0.346+j0.239	0.347+j0.238	$A_{1,15}$	-0.139+j0.352	-0.139+j0.352
$A_{1,4}$	0.346+j0.053	0.346+j0.053	$A_{1,16}$	0.057+j0.158	0.056+j0.158
$A_{1,5}$	-0.132+j0.014	-0.132+j0.014	$A_{1,17}$	0.008-j0.178	0.008-j0.178
$A_{1,6}$	0.269-j0.166	0.268-j0.167	$A_{1,18}$	0.001+j0.063	j0.063
$A_{1,7}$	-0.197+j0.067	-0.198+j0.068	$A_{1,19}$	-0.114-j0.027	-0.115-j0.027
$A_{1,8}$	-0.301-j0.599	-0.303-j0.598	$A_{1,20}$	0.120-j0.021	0.119-j0.021
$A_{1,9}$	-0.297-j0.126	-0.298-j0.126	$A_{1,21}$	-0.019+j0.109	-0.020+j0.110
$A_{1,10}$	0.101+j0.055	0.101+j0.056	$A_{1,22}$	-0.037-j0.021	-0.038-j0.021
$A_{1,11}$	0.067-j0.065	0.067-j0.065	$A_{1,23}$	-0.148	-0.148
$A_{1,12}$	-0.183-j0.078	-0.184-j0.078			

B. Reconstructed Power Spectrum Density

Assume there exist two BPSK modulated signal with the same symbol rate $s_r = 1\text{Mbaud}$ in the bandwidth of $[0,150\,\text{MHz}]$, the carrier of which are 46.67MHz and 126.67MHz respectively. We employ the MWC framework to accomplish compressed sampling and the number of sampling channel m is set as 10. The periodic pseudorandom waveform used in the i th channel is generated by cycling shifting the one in Fig. 4(a) with $(i-1)\times 10\text{ns}$. The corresponding pseudorandom sequence will be cycling shifted with 3 bits. After compressed sampling, the original signal is reconstructed by using measurement matrix from both proposed method and theorem.

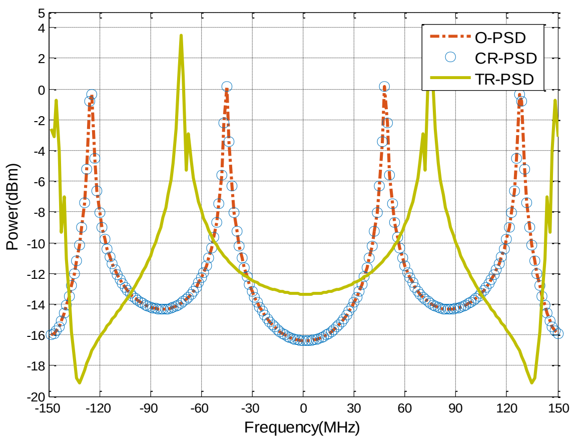

Fig. 6. Reconstructed PSD and original PSD

Fig. 6 compares the power spectrum density of original signal with that of reconstructed signal via both FWC method and theoretical method that does not calibrate the measurement matrix. As is shown in Fig. 6, the recovered power spectrum density CR-PSD by using the calibrated measurement matrix matches perfectly with the original signal power spectrum density O-PSD, while the recovered power spectrum density TR-PSD by using theory computation without calibration differs greatly with the true O-PSD. Accordingly, it is necessary and vital to do calibration on the measurement matrix when using MWC framework and this also verifies the validity of the proposed FWC method.

C. Correct Recovery Ratio of the Support

Similar to subsection B, given two BPSK modulated signal with the same symbol rate $s_r = 1\text{Mbaud}$ within the bandwidth of $[0,150\,\text{MHz}]$, the carrier frequency of them are set randomly under the constraint that these two signals will not alias each other in frequency domain, and the total power of the two signals is P watt. The double-sideband power spectrum density of white noise is assumed to be $n_0 = 10^{-10}\,\text{W/KHz}$ within the equivalent bandwidth, therefore the noise power is $N_0 = n_0 f_{NYQ}$. The signal to noise ratio defined as $SNR = 10\log10(P / N_0)$ varies from -5dB to 30dB. Adopt MWC framework to acquire signal samples and OMP optimization algorithm to recover the support. If the recovered support is consistent with the support of the original signal, it is regarded as a successful recovery otherwise the recovery failed. Via Monte Carlo method, we conduct 1000 simulations and record the number of correct recovery, obtaining the percentage of successful support recovery ratio which is plotted in Fig. 7.

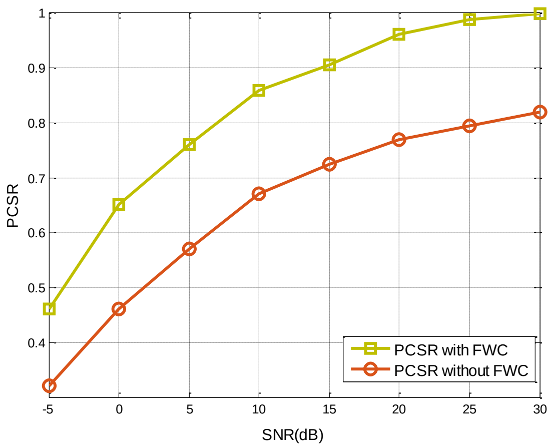

Fig. 7. Correct recovery ratio with different methods

Fig. 7 shows obviously that the successful recovery ratio using calibrated measurement matrix outperforms that obtained from theory measurement matrix without calibration in a wide range of SNR. The maximum difference of these two results can be as large as 20%. According to the results of Fig. 6 and Fig. 7, it can be concluded that utilizing FWC method to calibrate the measurement matrix improves the correct recovery ratio of signal support and obtains reconstructed signal that is highly matched with the original signal. This is of great concern for MWC compressed sampling framework that it can be more practical in the application of cognitive radio, UWB electronic reconnaissance and some other electronic countermeasures systems.

VI. Conclusion

In this paper, we proposed a Full-column-rank Well Posed Calibration (FWC) algorithm, along with its detailed theory foundation to deal with the mismatch problem in practical implementation of MWC framework. It aims at calibrating the measurement matrix and improving the correct ratio of recovering signals. Analysis and numerical simulation show that the measurement matrix obtained by FWC method is highly consistent with the one that is calculated through the FFT of the periodic pseudorandom waveform. And the accuracy of the reconstructed signal by using the proposed algorithm outperforms that by using conventional theory method without calibration.

References

[1] C. E. Shannon, “Communication in the presence of noise,” *Proceedings of the IRE*, vol. 37, no. 1, pp. 10-21, Jan. 1949.

[2] S. Qaisar, R. M. Bilal, W. Iqbal, M. Naureen, and S. L. Lee, “Compressive sensing: From theory to applications, a survey,” *Journal of Communications and Networks*, vol. 15, no. 5, pp. 443-456, Oct. 2013.

[3] Y. H. Chen, H. J. Wan, and S. B. Zhang, “Opportunistic spectrum access in imperfect spectrum sensing cognitive networks,” *Journal of Communications*, vol. 10, no. 6, pp. 410-414, June 2015.

[4] Y. Liu, Z. D. Zhong, G. P. Wang, and D. Hu, “Cyclostationary detection based spectrum sensing for cognitive radio,” *Journal of Communications*, vol. 10, no. 1, pp. 74-79, Jan. 2015.

[5] S. X. Yin, D. W. Chen, and Q. Zhang, “Mining spectrum usage data: A large-scale spectrum measurement study,” *IEEE Trans. on Mobile Computing*, vol. 11, no. 6, pp. 1033-1046, June 2012.

[6] N. Tong and L. C. Li, “Correlation-Index blind classification for MFSK with unreconstructed compressive samplings,” *Journal of Communications*, vol. 10. no. 7, pp. 544-550, July 2015.

[7] D. L. Donoho, “Compressed sensing,” *IEEE Trans. on Information Theory*, vol. 52, no. 4, pp. 1289-1306, April 2006.

[8] N. T. Son, N. V. Quynh, P. V. Toan, and L. P. Truong, “Compressed sensing: A new approach to analyze the recovery algorithms based on UWB channel estimation”, in *Proc. International Conference on Computing, Management and Telecommunications*, Da Nang, 2014, pp. 27-29.

[9] S. Kirolos, J. Laska, M. Wakin, M. Duarte, *et al.*, “Analog-to-Information conversion via random demodulation,” presented at the IEEE Dallas/CAS Workshop on Design, Applications, Integration and Software, Richardson, TX, 2006, pp. 71-74.

[10] J. N. Laska, S. Kirolos, M. F. Duarte, T. S. Ragheb, R. G. Baraniuk, and Y. Massoud, “Theory and implementation of an analog-to-information converter using random demodulation,” in *Proc. IEEE International Symposium on Circuits and Systems*, New Orleans, LA, 2007, pp. 1959-1962.

[11] J. Romberg, “Compressive sensing by random convolution,” *SIAM Journal on Imaging Sciences*, vol. 2, no. 4, pp. 1098-1128, 2009.

[12] C. H. Lin, S. H. Tsai, and G. C. H, Chuang, “A novel Sub-nyquist sampling of sparse wideband signals,” in *Proc. IEEE International Conference on Acoustics, Speech and Signal Processing*, Vancouver, BC , 2013, pp. 4628-4632.

[13] M. Mishali and Y. C. Eldar, “From theory to practice: Sub-Nyquist sampling of sparse wideband analog signals,” *IEEE Journal of Selected Topics in Signal Processing*, vol. 4, no. 2, pp. 375-391, Feb. 2010.

[14] M. Mishali and Y. C. Eldar, “Blind multiband signal reconstruction: Compressed sensing for analog signals,” *IEEE Trans. on Signal Processing*, vol. 57, no. 3, pp. 993-1009, Jan. 2009.

[15] M. Mishali, Y. C. Eldar, and A. J. Elron, “Xampling: Signal acquisition and processing in union of subspaces,” *IEEE Trans. on Signal Processing*, vol. 59, no. 10, pp. 4719-4734, July 2011.

[16] M. Mishali, Y. C. Eldar, O. Dounaevsky, and E. Shoshan, “Xampling: Analog to digital at sub-Nyquist rates,” *IET Circuits, Devices & Systems*, vol. 5, no. 1, pp. 8-20, Jan. 2011.

[17] Y. L. Chen, M. Mishali, Y. C. Eldar, and A. O. Hero, “Modulated wideband converter with non-ideal lowpass filters,” in *Proc. IEEE International Conference on Acoustics Speech and Signal Processing*, Dallas, TX, 2010, pp. 3630-3633.

[18] B. Eric, *Signal Integrity: Simplified*, 3rd ed. Upper Saddle River: Prentice Hall Professional, 2004, pp. 162.

Tian-Yi Xiong was born in Sichuan Province, China, in 1989. He received the B.S. degree in optical information science and technology from South China University of Technology (SCUT), Guangzhou, in 2011. He is currently pursuing the Ph.D. degree in the School of Telecommunications Engineering, Xidian University. His research interests include wireless communication, spectrum sensing and cognitive radio networks.

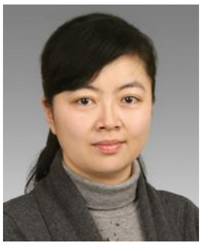

Zan Li was born in Shaanxi Province, China, in 1975. She received the B.S. degree in Telecommunications Engineering, M.S. degree and Ph.D. degree in Communication and Information system from Xidian University. She is now a professor in the School of Telecommunications Engineering in Xidian University. Her research interests include wireless communication system, cognitive radio networks and digital signal processing.

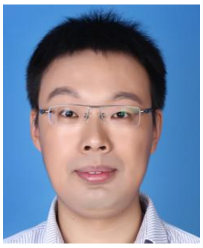

Pei-Han Qi was born in Henan Province, China, in 1986. He received B.S. degree in Telecommunications Engineering from Chang'an University, Xi'an, in 2006, the M.S. degree in communication and information system from Xidian University, in 2011 and Ph.D. degree in military communication from Xidian University, in 2014. Since Jan. 2015, he has been a post doctor in the School of Telecommunications Engineering in Xidian University. He is interested in compressed sensing, spectrum sensing in cognitive radio networks and high speed digital signal processing.